

Shear fracture behavior of Ti_3SiC_2 induced by compression at temperatures below 1000°C

Z.F. Zhang^{a,b,*}, Z.M. Sun^b

^a *Shenyang National Laboratory for Materials Sciences, Institute of Metal Research, Chinese Academy of Sciences, 72 Wenhua Road, Shenyang 110016, PR China*

^b *AIST Tohoku, National Institute of Advanced Industrial Science and Technology, 4-2-1, Nigatake, Miyagino-ku, Sendai 983-8551, Japan*

Received in revised form 14 July 2005; accepted 26 July 2005

Abstract

Polycrystalline titanium silicon carbide (Ti_3SiC_2) samples with grain size of 20–50 μm were synthesized from 2Ti/2Si/3TiC powder at 1300°C for 60 min through the pulse discharge sintering (PDS) technique. Compressive tests were conducted on the Ti_3SiC_2 specimens at temperatures up to 930°C in vacuum. The results showed that the Ti_3SiC_2 specimens displayed obvious shear fracture behavior and monotonically decreasing fracture strength from 935 MPa (25°C) to 640 MPa (930°C). On the macro-scale, the shear fracture surfaces make an angle of $23\text{--}31^\circ$ with respect to the stress axis. In micro-scale, the main deformation and damage modes consist of sliding, buckling and fracture of grains, kinking and intergranular cracking. The macro-shear fracture mechanism of Ti_3SiC_2 is quite analogous to other brittle materials, such as polycrystalline ice and bulk metallic glasses (BMGs). Based on the results available, the shear fracture mechanism of Ti_3SiC_2 is discussed and related to the behavior of other brittle materials.

© 2005 Elsevier B.V. All rights reserved.

Keywords: Ti_3SiC_2 ; Deformation and damage; Shear fracture; Fracture angle

1. Introduction

Titanium silicon carbide (Ti_3SiC_2) is one of several novel materials with properties unique to both metals and ceramics [1]. Recently, Ti_3SiC_2 - or Ti_3SiC_2 -based materials were synthesized by a number of different techniques [2–8] and were widely investigated to determine, for example, indentation hardness [2,4,6,9–12], compression [4,6,8,10,13–17], bending [4,6,8,10,16,18] and tension properties [8,10,19,20]. Normally, Ti_3SiC_2 can display several deformation and damage mechanisms, such as sliding, kinking, buckling or delamination and intergranular cracking under different loading modes [9–20]. Barsoum and El-Raghy [1,9,10,13,14,19,20] systematically investigated the compressive, flexure and tensile deformation behavior of fine and coarse-grained Ti_3SiC_2 with high purity (~ 98 wt%) fab-

ricated from Ti/SiC/C powders by a hot isotropic pressing (HIP) technique. They found a brittle-to-ductile transition at 1200°C with significant plasticity (20%) prior to failure [19]. Above 1200°C , Ti_3SiC_2 can deform in a pseudo-plastic manner with significant ductility. At 1300°C , its “yield” strengths in flexure and compression were found to be 100 MPa and 500 MPa, respectively. When some large-grained (1–3 mm), oriented, polycrystalline Ti_3SiC_2 samples were subjected to compression at room temperature, substantial plasticity ($>20\%$) occurred by a combination of the delamination of individual grains and the formation of shear and kink bands [13,14]. Recently, Sun et al. [17] found an anomalous positive temperature dependence of flow stress for the first time in polycrystalline Ti_3SiC_2 samples with low purity (87 wt% and 93 wt%) fabricated from Ti/Si/C powders through reactive sintering technique. They attributed the anomalous flow stress to the change in the deformation mechanisms with increasing testing temperature. Apparently, the mechanical properties of Ti_3SiC_2

* Corresponding author. Tel.: +86 24 23971043; fax: +86 24 23891320.
E-mail address: zhzhzhang@imr.ac.cn (Z.F. Zhang).

depend strongly on the starting powders (such as Ti/Si/C and Ti/SiC/C), synthesis method, purity and microstructure in detail.

On the other hand, Ti_3SiC_2 is typical brittle material in the low temperature range and is comparable to materials, such as polycrystalline ice [21–29] and bulk metallic glasses (BMGs) [30–39]. There are abundant mechanical property data for these two types of materials. Barsoum et al. [29] compared the brittle and ductile failure behavior of polycrystalline ice and Ti_3SiC_2 samples for the first time. They summarized that, to some extent, the deformation responses of Ti_3SiC_2 and ice are quite similar, i.e. strain-rate sensitive. At high strain rate, they are brittle, however, become quite plastic at low strain rate. Meanwhile, there exists key difference in the deformation and fracture mechanisms between the two materials. BMGs and their composites are newly developed and have attracted extensive attention in recent years [30,31]. They often display shear fracture with extremely high strength and the existence of ductility or not strongly depends on compositional or microstructural details [32–39]. However, the deformation and shear fracture mechanisms of these three types of brittle materials have never been compared.

In our recent work, Ti_3SiC_2 samples with high purity (~99 wt%) were synthesized from Ti/Si/TiC powders through a pulse discharge sintering (PDS) technique in a temperature range of 1250–1300 °C, which is about 200–300 °C lower than the sintering temperature by HIP from Ti/Si/C or Ti/SiC/C powders [40–42]. These Ti_3SiC_2 samples displayed very high plasticity at temperatures over 1200 °C when subjected to bending loads [40]. In the present investigation, compressive tests of Ti_3SiC_2 specimens will be carried out in a relatively low temperature range (below 1000 °C), so that a typical brittle failure mode is expected, as in BMGs and polycrystalline ice. We will further reveal the compressive deformation and shear fracture behavior of Ti_3SiC_2 samples as well as polycrystalline ice and BMGs.

2. Experimental procedure

Commercially available Ti (10 μm and 99.9%), Si (10 μm and 99.9%) and TiC (2–5 μm and 99%) powders with a molar ratio of 2:2:3 were selected for the present research. The molar ratio 2:2:3 of Ti:Si:TiC powder mixture was employed for optimizing the Ti_3SiC_2 purity, as reported elsewhere [41]. Before sintering, the powder was mixed by a Turbula shaker mixer in Ar atmosphere for 24 h, then was compacted into a graphite mold (50 mm in diameter) and sintered in vacuum (10^{-4} Pa) at 1300 °C for 60 min using the PDS technique. The heating rate was controlled at 50 °C/min and the applied pressure was maintained constant at 50 MPa during sintering. After sintering, the surfaces of the samples were ground to remove the graphite layer and analyzed by X-ray diffractometry (XRD) with Cu $K\alpha$ radiation at 30 kV and

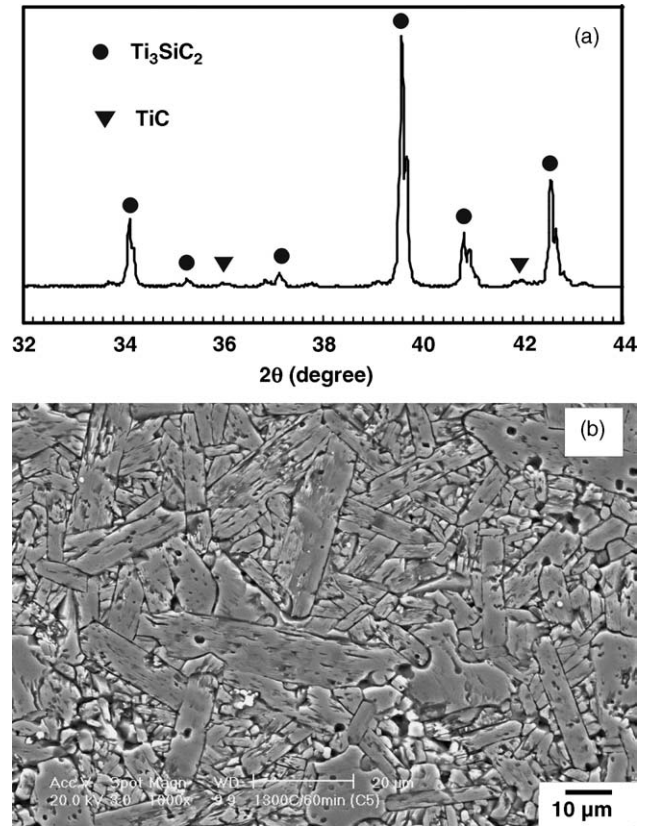


Fig. 1. (a) X-ray diffraction profiles and (b) microstructure of Ti_3SiC_2 samples sintered from 2Ti/2Si/3TiC powder mixture at 1300 °C for 60 min through pulse discharge sintering (PDS) technique.

40 mA to show the composition phases. Fig. 1(a) gives the X-ray diffraction profile of the sintered bulk Ti_3SiC_2 sample scanned at $2\theta = 32\text{--}44^\circ$. It can be seen that both main and second peaks of the TiC impurity show a low diffraction intensity even at a slow scanning rate of $0.02^\circ \text{ s}^{-1}$. Other than this, all the peaks correspond to the Ti_3SiC_2 phase. By the standard additive method [41], the purity of Ti_3SiC_2 in the sintered samples was calculated to be about 99 wt% with residual TiC impurity from its XRD data in Fig. 1(a). Microstructure observations by scanning electron microscopy (SEM) showed that the Ti_3SiC_2 grains have a lath-like structure with a length range of 20–50 μm , as shown in Fig. 1(b). This microstructure is similar to the duplex-phase grains fabricated by El-Raghy and Barsoum [5]. The compressive specimens were cut by an electron-spark cutting machine from the sintered bulk Ti_3SiC_2 disk with a dimension of 50 mm and 3 mm in thickness. Then, all the specimens were mechanically polished to a dimension of 2.5 mm \times 2.5 mm \times 6 mm with smooth surfaces for microscopic observation. The compressive tests were performed with an Instron 8562 servo-hydraulic testing machine under a constant strain rate of $6 \times 10^{-4} \text{ s}^{-1}$ in a temperature range of 25–930 °C in vacuum. After failure, all specimens were observed by SEM to reveal the deformation and damage features.

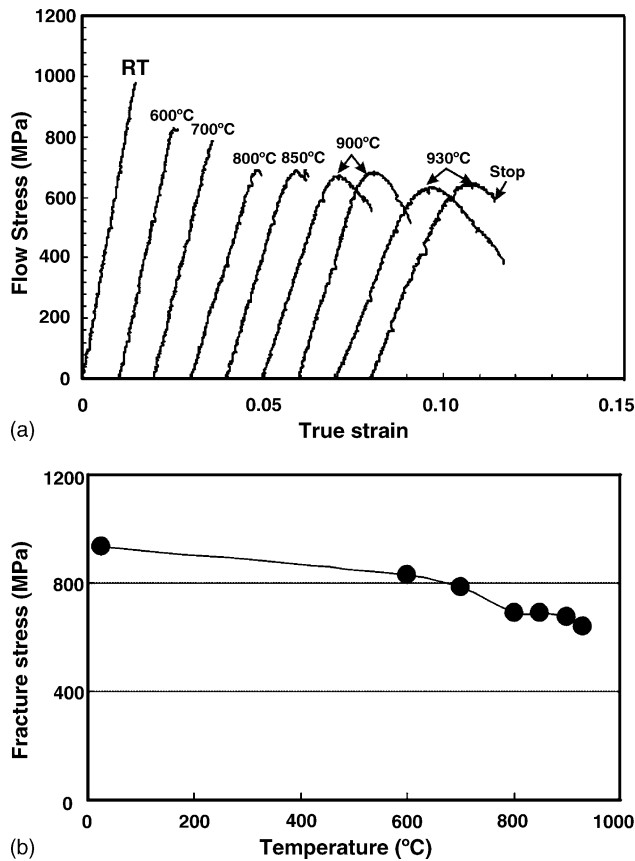


Fig. 2. (a) True compressive stress–strain curves below 1000 °C and (b) dependence of fracture strength on the testing temperature for the Ti_3SiC_2 specimens.

3. Experimental results

3.1. Compressive stress–strain curves

Fig. 2(a) shows the true compressive stress–strain curves of the Ti_3SiC_2 specimens at various temperatures. For comparison, some curves are shifted a strain of 1% to the right. It can be seen that the Ti_3SiC_2 specimens display elastic deformation behavior, and consequent abrupt brittle fracture at testing temperatures below 800 °C. Over 850 °C, the compressive plasticity increases with increasing temperatures. This indicates that the brittle-to-ductile transition temperature for the present Ti_3SiC_2 specimens occurs near 850 °C. However, for the TSC^{Z610} and TSC^{Z510} specimens fabricated from Ti/Si/C powder [15–17], the plastic deformation could only be observed at temperatures above 1050 °C, which is distinctly higher than the present transition temperature. For the Ti_3SiC_2 samples fabricated by Ti/SiC/C powder [10], the brittle-to-ductile transition temperature occurred around 1100–1200 °C. Fig. 2(b) demonstrates the dependence of compressive fracture strength σ_F on the testing temperature for the present Ti_3SiC_2 specimens. The fracture strength σ_F shows a high value of 935 MPa at room temperature, but decreases to 640 MPa at 930 °C. This fracture strength is

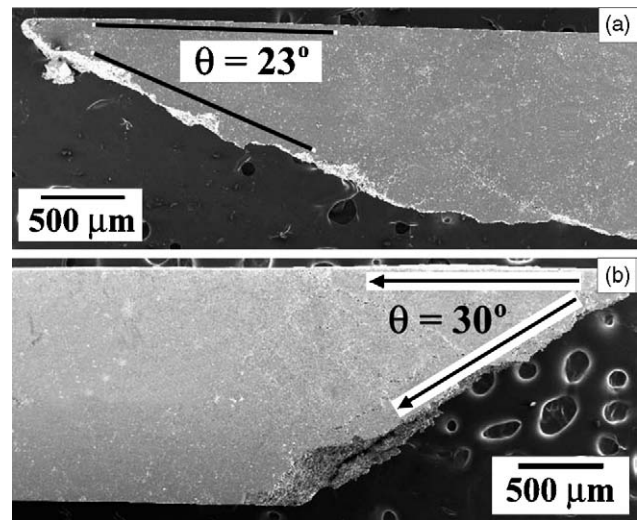


Fig. 3. Shear fracture feature of Ti_3SiC_2 specimens at: (a) room temperature (25 °C) and (b) 900 °C.

comparable to the data of Li et al. [8], El-Rahgy et al. [10] and Zhou and Sun [15–17]. However, the anomalous positive temperature dependence of flow stress in the present tests was not observed as reported by Sun et al. [17].

3.2. Macro-scale shear fracture features

After failure, it is noted that most Ti_3SiC_2 specimens fractured in a shear mode and were broken into two parts, as shown in Fig. 3(a and b). The fracture surfaces make an angle θ_C with the stress axis, as marked in Fig. 3. Over the testing temperatures (25–930 °C), the shear fracture angle θ_C was found to be in the range of 23–31°, which deviates from the maximum shear stress plane (45°). This macro-scale shear fracture behavior has been widely observed in some brittle materials, such as polycrystalline ice [21–27] and bulk metallic glassy materials [32–39], as listed in Table 1. This indicates that the shear fracture behavior of these three types of brittle materials does not obey the Tresca fracture criterion [32]. In comparison with the fully metallic glasses [32–36], the fracture surfaces of Ti_3SiC_2 specimens are relatively rough and are quite similar to polycrystalline ice [22–24] and metallic glassy composites [37–39]. Meanwhile, it is noted that the shearing did not penetrate through the whole Ti_3SiC_2 specimen at room temperature, but changes its path to a plane basically parallel to the stress axis, as shown in Fig. 3(a). At high temperature, the shearing can well pass through the whole section of the Ti_3SiC_2 specimen, as shown in Fig. 3(b). This demonstrates that testing temperature also affects the failure process and the orientation of the shear fracture plane for Ti_3SiC_2 specimens.

3.3. Micro-scale deformation and damage features

At temperatures below 800 °C, no obvious plastic deformation can be observed on any of the specimen surfaces. A

Table 1
Comparison of the compressive fracture angle θ_C for different brittle materials

Material types	Investigators	Compositions	Microstructure	Fracture angle ($^\circ$)
Ice	Schulson [25]	H ₂ O (ice)	Polycrystalline	~30
	Renshaw and Schulson [26]	H ₂ O (ice)	Polycrystalline	~30
	Kirchner et al. [27]	H ₂ O (ice)	Polycrystalline	28–30
Amorphous materials	Donovan [32]	Pd ₄₀ Ni ₄₀ P ₂₀	Amorphous	41.9 ± 1.2
	He et al. [33]	Zr _{52.5} Ni _{14.6} Al ₁₀ Cu _{17.9} Ti ₅	Amorphous	40–45
	Lowhaphandu et al. [34]	Zr ₆₂ Ti ₁₀ Ni ₁₀ Cu _{14.5} Be _{3.5}	Amorphous	41.6 ± 2.1
	Wright et al. [35]	Zr ₄₀ Ti ₁₄ Ni ₁₀ Cu ₁₂ Be ₂₄	Amorphous	~42
	Zhang et al. [36]	Zr ₅₉ Cu ₂₀ Al ₁₀ Ni ₈ Ti ₃	Amorphous	~43
	Zhang et al. [37]	Zr _{52.5} Ni _{14.6} Al ₁₀ Cu _{17.9} Ti ₅	Amorphous	~42
	He et al. [38]	(Zr _{0.55} Cu _{0.30} Al _{0.10} Ni _{0.05}) ₁₋₉₅ Ta ₅	BMG + Ta particles	~32
	Zhang et al. [39]	Ti ₅₀ Cu ₂₂ Ni ₂₀ Sn ₃ Si ₂ B ₃	BMG + dendritic phase	~32
	Zhang et al. [37]	Ti ₅₆ Cu _{16.8} Ni _{14.4} Sn _{4.8} Nb ₈	BMG + dendritic phase	~27
Ceramic	Present results (25–930 °C)	Ti ₃ SiC ₂	Polycrystalline	23–31

few cracks and local damage are shown in Fig. 4(a and b). The fracture has localized into one main crack and failed in a shear mode. Normally, the deformation and damage of the Ti₃SiC₂ specimens consists mainly of intergranular cracking (Fig. 4(a)), fracture of grains and local cracking (Fig. 4(b)). Therefore, there is little contribution to plasticity during compressive deformation at low testing temperatures. This is consistent with previous reports in other Ti₃SiC₂ testing [5,6,8,10,16].

Over 900 °C, the deformation and damage are observed to be relatively homogenous after failure of Ti₃SiC₂ specimens. As shown in Fig. 4(c), multiple micro-cracks and local deformation are much more homogeneously distributed on the specimen surface. Sliding, intergranular cracking, kinking, buckling and fracture of grains prevail within the deformation and damage regions. Therefore, the obvious plastic deformation over 900 °C can be attributed to a relatively homogenous distribution of sliding, intergranular cracking,

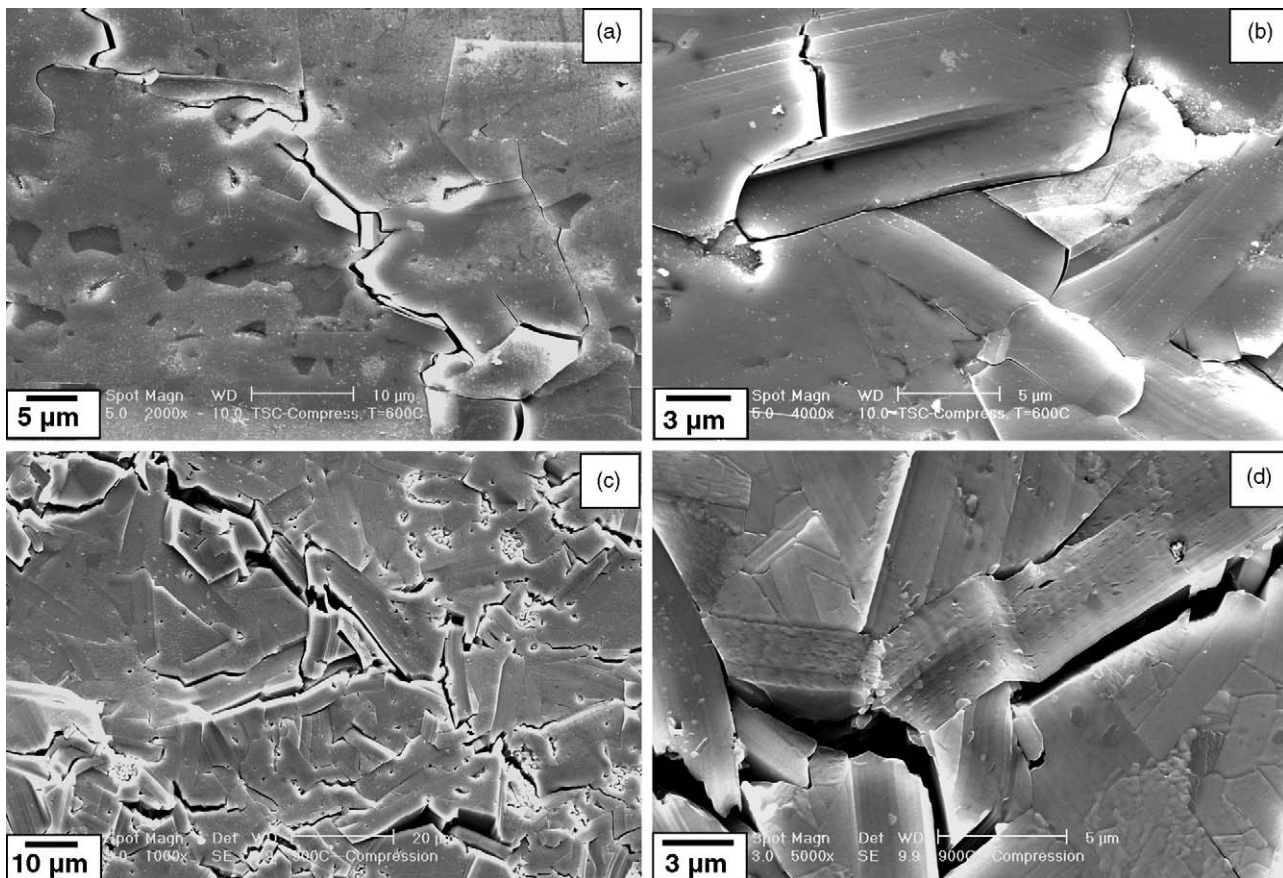


Fig. 4. Surface deformation morphology of Ti₃SiC₂ specimens at different temperatures: (a and b) room temperature and (c and d) 900 °C.

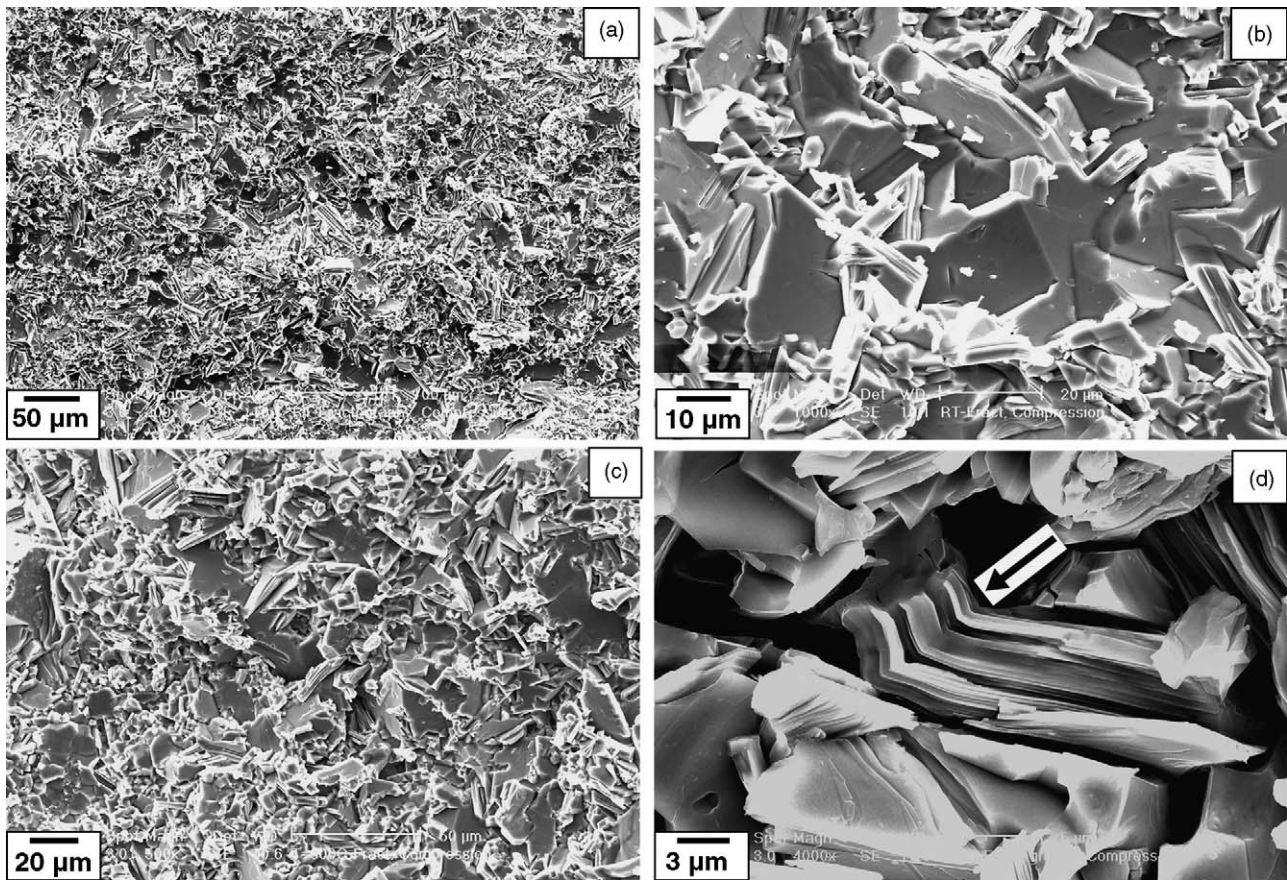


Fig. 5. Fracture surface morphology of the Ti_3SiC_2 specimens at different temperatures: (a and b) room temperature and (c and d) 900°C .

kinking, buckling and fracture of grains. Another interesting feature is that kink bands can be frequently observed at high temperature (see Fig. 4(d)). Although these kink bands themselves cannot accommodate much plastic strain, they can change the orientation of Ti_3SiC_2 grains, and in turn, play an important role in coordinating the plastic deformation process at high temperature. Therefore, the plasticity observed in stress–strain curves can be explained by the action of multiple deformation and damage modes, which is obvious pseudo-plastic behavior, as pointed out by Radovic et al. [19].

3.4. Fractography observations

Fractography observations showed that the shear fracture surfaces are relatively rough, as shown in Fig. 5(a and c). At high magnification, some flat steps or facets can be clearly seen (Fig. 5(b)). These flat steps or facets are attributed to the local cleavage fracture of Ti_3SiC_2 grains or intergranular cracking. At high temperature, the fractography shows a similar feature with those at low temperature (see Fig. 5(c)). However, kinking is still frequently observed on fractography, as indicated by the arrow in Fig. 5(d). This is identical with the surface deformation morphologies in Fig. 4(d), providing further evidence for the kinking of Ti_3SiC_2 at high

temperatures. While, for other brittle materials, such as polycrystalline ice and BMGs, shear fracture surfaces are always accompanied by melting [22–24,32–39], Ti_3SiC_2 shows no sign of melting during shear fracture. For fully amorphous alloys, shear fracture surfaces are always very smooth or flat with the formation of a vein-like structure [32–36]. In polycrystalline ice, Ti_3SiC_2 and BMG composites [37–39], relatively rough fracture surfaces can be attributed to the deviation of local shear cracking across grain boundaries or grains.

4. Discussion

The deformation and fracture behavior of Ti_3SiC_2 have been widely investigated by several research groups in recent years [9–20]; however, there is no report about shear fracture. For some brittle materials, such as BMGs and polycrystalline ice, it is frequently observed that their shear fracture surfaces often deviate from the maximum shear stress plane under compression (see Table 1) [25–27,32–39]. The present results ($\theta_C = 23\text{--}31^\circ$) in Ti_3SiC_2 specimens are identical with observations in these other materials. Therefore, the macro-shear fracture mechanisms for these three brittle materials should, to some extent, be quite similar and should be described using

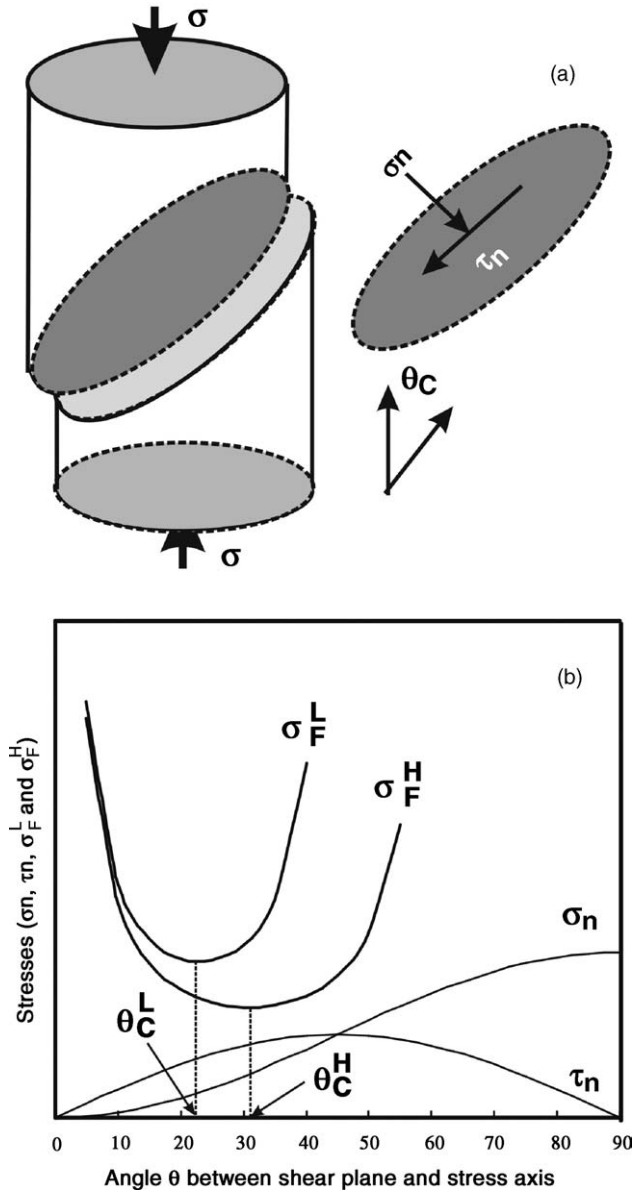


Fig. 6. Illustration of: (a) stress distribution on any shear plane and (b) variation of compressive fracture stresses σ_F^L and σ_F^H at low and high temperatures, normal stress σ_n and shear stress τ_n with shear angle θ under compressive loading.

a Mohr–Coulomb criterion [37], i.e.

$$\tau_n + \mu \cdot \sigma_n \geq \tau_C \quad (1)$$

Here, μ is a constant for a brittle material and τ_C is the critical shear fracture stress. As shown in Fig. 6(a), τ_n and σ_n are shear stress and normal stress on any shear plane and can be expressed as below:

$$\sigma_n = \sigma \cdot \sin^2(\theta) \quad (2a)$$

$$\tau_n = \sigma \cdot \sin(\theta) \cdot \cos(\theta), \quad (2b)$$

where σ is the applied compression stress and θ is the interaction angle between stress axis and shear plane. Substituting

σ_n and τ_n into Eq. (1) yields the critical fracture condition for Ti_3SiC_2 as

$$\sigma_F \geq \frac{\tau_C}{\sin(\theta) \cdot [\cos(\theta) - \mu \cdot \sin(\theta)]} \quad (3)$$

where σ_F is the applied compressive stress at shear fracture. From Eq. (3), it is apparent that σ_F depends strongly on the shear angle θ , and can be schematically illustrated as in Fig. 6(b). σ_F^L and σ_F^H demonstrate the variation of fracture strength, σ_F , with shear angle, θ , at low and high temperatures. It is natural that a specimen must fracture along a favorable shear plane at the minimum fracture stress σ_F , which is taken to correspond to the measured, θ_C , according to the following equation:

$$\frac{\partial(1/\sigma_F)}{\partial\theta} = \frac{1}{2\tau_C} [\cos(2\theta_C) - \mu \cdot \sin(2\theta_C)] = 0 \quad (4)$$

Therefore, the critical shear fracture condition can be expressed as

$$\mu = \frac{\cos(2\theta_C)}{\sin(2\theta_C)} = c \tan(2\theta_C). \quad (5)$$

Furthermore, from Eqs. (3)–(5), τ_C can be calculated by the following equation:

$$\tau_C = \sigma_F \cdot \sin(\theta_C) \cdot [\cos(\theta_C) - \mu \cdot \sin(\theta_C)]. \quad (6)$$

The macro-shear fracture stress τ_C represents the average resistance to break a polycrystalline Ti_3SiC_2 specimen through intergranular cracking and fracture of grains. In Fig. 6(b), θ_C^L and θ_C^H represent the measured fracture angles θ_C at low and high temperatures. At $T = 25^\circ\text{C}$, $\theta_C^{25} = 23^\circ$, and for $T = 930^\circ\text{C}$, $\theta_C^{930} = 31^\circ$; therefore, from Eq. (5), one can calculate the constant μ as $\mu^{25} = 0.966$ and $\mu^{930} = 0.532$, respectively. According to the data above and Eq. (6), we can compute $\tau_C^{25} = 198\text{ MPa}$ and $\tau_C^{930} = 192\text{ MPa}$, respectively. It can be seen that τ_C is approximately in the range of 192–198 MPa at the testing temperatures. It means that the Ti_3SiC_2 specimen can be sheared to fracture by a constant pure shear stress around $\sim 195\text{ MPa}$, which is obviously higher than the critical resolved shear stress of 36 MPa on the basal plane of coarse-grain (1–3 mm) Ti_3SiC_2 specimens [13]. The increase in τ_C can be attributed to a relatively smaller grain size (20–50 μm) in the present Ti_3SiC_2 specimens.

For the BMG materials and polycrystalline ice, their θ_C also shows a similar feature (see Table 1). The difference is that θ_C in the fully amorphous alloys is around $42\text{--}43^\circ$, quite close to 45° . However, in polycrystalline materials, their shear fracture angles deviate from the maximum shear stress plane more significantly, such as in ice ($\theta_C = 30^\circ$), BMG composites ($\theta_C = 27^\circ, 32^\circ$) and the present Ti_3SiC_2 ($\theta_C = 23\text{--}31^\circ$). This indicates that the grain size or distribution can strongly affect the orientation of the shear fracture plane and the normal stress σ_n plays a more significant role in the shear fracture of brittle polycrystalline materials.

Since the average critical macro-shear fracture stress τ_C is nearly a constant, from Eq. (5), it is clear that $\theta_C^L < \theta_C^H$ leads to $\mu^L > \mu^H$. From Eq. (7), it is easy to understand why the fracture strength σ_F^L at low temperature is always higher than σ_F^H at high temperature. The decrease in the fracture strength of Ti_3SiC_2 specimens can be attributed to the change in θ_C or μ with increasing testing temperature. On the micro-scale, it has been observed that not only the formation of kinking, but also the homogeneous distribution of deformation and damage tend to occur at high temperature, as shown in Fig. 4. It is apparent that the two deformation mechanisms will be beneficial to the plasticity of Ti_3SiC_2 at high temperature. Meanwhile, kinking can change the orientation of the Ti_3SiC_2 grains and furthermore, modify the propagation path of shear cracking locally. In other words, the homogeneous distribution of deformation and damage at high testing temperature will make shear cracking more close to the maximum shear stress plane.

As widely observed, the shear fracture of polycrystalline ice and BMG materials is always accompanied by melting, as evidenced by fractography [22–24,32–39]. Recently, Wright et al. [35] analyzed the melting phenomenon induced by shear fracture in BMGs. They found that the increase in temperature within the shear band is as high as 900 K, which is sufficient to melt the BMG locally. For all BMG materials, their melting points are modest (around 1000 °C) [35]; however, their fracture strengths can reach ~2000 MPa [32–39]. For Ti_3SiC_2 specimens, melting phenomenon has never been observed even at testing temperatures over 1400 °C, because it has a very high melting point of ~3000 °C. Barsoum et al. [29] pointed out that polycrystalline ice fails mostly in a brittle manner even though the testing temperature is close to its melting point. By contrast, Ti_3SiC_2 specimens can display obvious plasticity at temperatures far below its melting point. It is well known that the melting point of a material correlates with hardness or strength. According to the estimation by Wright et al. [35], one can in return calculate the limiting fracture strength of Ti_3SiC_2 , σ_F^m , which induces local melting during shear fracture. The melting points ($T_m = \sim 3000$ °C), elastic modulus ($E = 325$ GPa), heat capacity ($C_p = 588$ J/(kg K)) and density ($\rho = 4.53$ g/cm³) are known, so that σ_F^m is computed from

$$\sigma_F^m = \sqrt{2\alpha \cdot E \cdot \rho \cdot C_p \cdot \Delta T}. \quad (7)$$

Here, ΔT is the temperature difference between the melting point and testing temperature and α represents the ratio of the thickness of the shear layer to the whole specimen. Here, assuming $\alpha = 1\%$, the same as the evaluated value in BMG [35]. From Eq. (7), it is easy to calculate that σ_F^m for Ti_3SiC_2 is about 7.2 GPa, which is seven times higher than the actual fracture strength (~1 GPa). This means that σ_F^m is extremely high, at the point where the fracture can induce the local melting in Ti_3SiC_2 . Actually, for most materials, it is impossible, or at least difficult, to induce local melting during fracture. Polycrystalline ice and BMG materials can be regarded as

two types of special materials, which can fully exhibit their strength potential even to their melting point during fracture. In this sense, the great difference between σ_F and σ_F^m indicates that Ti_3SiC_2 still has great potential for improvement of strength by microstructure optimization through advanced sintering or fabrication techniques.

5. Conclusions

Based on the experimentally obtained results, the following conclusions can be drawn:

1. Under compressive loading, polycrystalline Ti_3SiC_2 samples synthesized from 2Ti/2Si/3TiC powder displayed brittle shear fracture behavior below 800 °C; however, over 850 °C, unmistakable plasticity can be observed. The fracture strength of the Ti_3SiC_2 samples monotonically decreased from 935 MPa to 640 MPa with increasing testing temperature.
2. The fracture of Ti_3SiC_2 originates mainly from one major crack and propagates along it, resulting in abrupt shear failure at temperatures below 930 °C. The macro-scale shear fracture angle ranges from 23° to 31°, indicating that the Tresca fracture criteria is invalid for Ti_3SiC_2 , as for polycrystalline ice and BMG materials. There exists a macro-scale critical shear fracture stress of 192–198 MPa, independent of the testing temperatures.
3. The micro-damage modes of Ti_3SiC_2 consist of sliding, kinking, buckling and fracture of grains and intergranular cracking. The “plasticity” of Ti_3SiC_2 above 850 °C can be attributed to relatively homogenous distribution of deformation and damage, which include sliding, kinking, buckling, fracture of grains and intergranular cracking. It is observed that kinking is a common deformation mode at high temperatures.

Acknowledgments

This work was supported by the National Natural Science Funds of China (NSFC) under Grant No. 50401019 and the “Hundred of Talents Project” by the Chinese Academy of Sciences.

References

- [1] M.W. Barsoum, Prog. Solid State Chem. 28 (2000) 201–281.
- [2] T. Goto, T. Hirai, Mater. Res. Bull. 22 (1987) 1195–1201.
- [3] X. Tong, T. Okano, T. Iseki, T. Yano, J. Mater. Sci. 30 (1995) 3087–3090.
- [4] M.W. Barsoum, T. El-Raghy, J. Am. Ceram. Soc. 79 (1996) 1953–1956.
- [5] T. El-Raghy, M.W. Barsoum, J. Am. Ceram. Soc. 82 (1999) 2849–2854.
- [6] N.F. Gao, Y. Miyamoto, J. Mater. Sci. 34 (1999) 4385–4392.
- [7] Z.M. Sun, Y.C. Zhou, Scripta Mater. 41 (1999) 61–66.

- [8] J.F. Li, W. Pan, F. Sato, R. Watanabe, *Acta Mater.* 49 (2001) 937–945.
- [9] T. El-Raghy, A. Zavaliangos, M.W. Barsoum, S.R. Kalidini, *J. Am. Ceram. Soc.* 80 (1997) 513–516.
- [10] T. El-Raghy, M.W. Barsoum, A. Zavaliangos, S.R. Kalidindi, *J. Am. Ceram. Soc.* 82 (1999) 2855–2860.
- [11] It M. Low, S.K. Lee, B.R. Lawn, *J. Am. Ceram. Soc.* 81 (1998) 225–228.
- [12] It M. Low, *J. Eur. Ceram. Soc.* 18 (1998) 709–713.
- [13] M.W. Barsoum, T. El-Raghy, *Metall. Mater. Trans. A29* (1998) 363–369.
- [14] M.W. Barsoum, L. Farber, T. El-Raghy, *Metall. Mater. Trans. A29* (1998) 1727–1738.
- [15] Y.C. Zhou, Z.M. Sun, *Mater. Res. Innovations* 2 (1999) 360–363.
- [16] Y.C. Zhou, Z.M. Sun, *J. Eur. Ceram. Soc.* 21 (2001) 1007–1011.
- [17] Z.M. Sun, Y.C. Zhou, J. Zhou, *Philos. Mag. Lett.* 80 (2000) 289–294.
- [18] Z.F. Zhang, Z.M. Sun, H. Hashimoto, *Mater. Lett.* 57 (2003) 1295–1299.
- [19] M. Radovic, M.W. Barsoum, T. El-Raghy, J. Seidensticker, S. Wiederhorn, *Acta Mater.* 48 (2000) 453–459.
- [20] M. Radovic, M.W. Barsoum, T. El-Raghy, J. Seidensticker, S. Wiederhorn, W.E. Luecke, *Acta Mater.* 50 (2002) 1297–1306.
- [21] E.M. Schulson, *Acta Metall. Mater.* 38 (1990) 1963–1976.
- [22] T.R. Smith, E.M. Schulson, *Acta Metall. Mater.* 41 (1993) 153–163.
- [23] D. Iliescu, E.M. Schulson, *Acta Mater.* 50 (2002) 2163–2172.
- [24] E.M. Schulson, *Acta Mater.* 50 (2002) 3415–3424.
- [25] E.M. Schulson, *Eng. Fract. Mech.* 68 (2001) 1839–1887.
- [26] C.E. Renshaw, E.M. Schulson, *Nature* 412 (2001) 897–900.
- [27] H.O.K. Kirchner, G. Michot, H. Narita, T. Suzuki, *Philos. Mag. A81* (2001) 2161–2181.
- [28] J.J. Petrovic, *J. Mater. Sci.* 38 (2003) 1–6.
- [29] M.W. Barsoum, M. Radovic, P. Finkel, T. El-Raghy, *Appl. Phys. Lett.* 79 (2001) 479–481.
- [30] W.L. Johnson, *MRS Bull.* 24 (10) (1999) 42–56.
- [31] A. Inoue, *Acta Mater.* 48 (2000) 279–306.
- [32] P.E. Donovan, *Acta Metall.* 37 (1989) 445–456.
- [33] G. He, J. Lu, Z. Bian, D.J. Chen, G.L. Chen, G.H. Tu, G.J. Chen, *Mater. Trans.* 42 (2001) 356–364.
- [34] P. Lowhaphandu, L.A. Ludrosky, S.L. Montgomery, J.J. Lewandowski, *Intermetallics* 8 (2000) 487–492.
- [35] W.J. Wright, R. Saha, W.D. Nix, *Mater. Trans.* 42 (2001) 642–649.
- [36] Z.F. Zhang, J. Eckert, L. Schultz, *Acta Mater.* 51 (2003) 1167–1179.
- [37] Z.F. Zhang, G. He, J. Eckert, L. Schultz, *Phys. Rev. Lett.* 91 (2003) 045505.
- [38] G. He, Z.F. Zhang, W. Löser, J. Eckert, L. Schultz, *Acta Mater.* 51 (2003) 2383–2395.
- [39] Z.F. Zhang, G. He, J. Eckert, *Philos. Mag.* 85 (2005) 897–915.
- [40] Z.F. Zhang, Z.M. Sun, H. Hashimoto, *Adv. Eng. Mater.* 4 (2002) 864–868.
- [41] Z.F. Zhang, Z.M. Sun, H. Hashimoto, *Metall. Mater. Trans. A33* (2002) 3321–3328.
- [42] Z.F. Zhang, Z.M. Sun, H. Hashimoto, *J. Am. Ceram. Soc.* 86 (2003) 431–436.